

Document downloaded from:

<http://hdl.handle.net/10251/193623>

This paper must be cited as:

Madrid García, JA.; Yahaghi, E.; Mirzapour, M.; Movafeghi, A. (2022). Improved revealing of hidden structures and defects for historic art sculptures using poisson image editing. *Journal of Cultural Heritage*. 55:381-390. <https://doi.org/10.1016/j.culher.2022.04.002>



The final publication is available at

<https://doi.org/10.1016/j.culher.2022.04.002>

Copyright Elsevier

Additional Information

**Improved Revealing of hidden structure and defects for historic art
sculptures using Poisson Image Editing**

ABSTRACT

Radiography is a non-destructive tool and offers the acquisition of detailed information on the internal features of sculptures as a cultural heritage. However, radiographs contain different levels of blurriness mainly caused by the detection of scattered X-rays. Reduction of image blurriness provides improved contrast in targeted areas which enhances extraction of information from the selected regions and features of the radiographs. In this study, we applied a set of convolution methods to a group of radiographic images of historic sculptures. Radiographs of the objects were provided with the associated documentation from the collection of the Radiographic Inspection Laboratory of the Universitat Politècnica de València. The selection of the particular objects was based on the difference in the materials used in their construction i.e. the objects were made of wood, paper, or wax. The Poisson Image Editing (PIE) based on L_2 -norm was applied for image enhancement of digital radiography images. The results showed that the PIE method was effective in selective region enhancement of the radiographic image contrast enabling better visualization of the objects' internal structures. Application of the implemented algorithm enabled the conservators and radiographers involved in the study to improve the visualization of the sculptures' internal features and they achieved enhanced evaluation of the defects.

Keywords: Cultural heritage, Poisson image editing, sculpture radiography; internal structure, digital image processing.

1. INTRODUCTION

Insight into the internal structure of artistic and cultural objects could provide useful information in their preservation and any necessary restoration procedures [1-2]. Many radiographic methods could be used to achieve this goal non-destructively i.e. without damaging the artworks including for example neutron radiography, computed tomography (CT), and fluoroscopy [1,3], which are among the non-destructive methods. One of the important methods in this scope is x-ray radiography.

Photon radiography systems rely on the collection of attenuated x-rays traversing the objects of interest. Whilst in traditional radiography the image is recorded on radiography film, in digital radiography systems detection is either by flexible phosphor plates for post-acquisition laser aided reading i.e. computed radiography (CR), or by a flat panel of detectors i.e. digital radiography (DR) [4-7]; Schalm et al. have compared the limitations and advantages of the different approaches [3].

Some digital radiography systems offer simple image processing capability within their built-in software. However, the application of advanced mathematical algorithms for information extraction from the acquired images requires additional software. These have been reported widely in the literature and have been applied with varying success in spatial as well as frequency domains [4, 8-9].

Neghadarzadeh et al. implemented the wavelet-domain hidden Markov models to enhance radiographs of Samiran potteries [7], Yahaghi et al. have successfully applied the dual-domain technique to radiographic images of art objects [10] and Morigi et al. used the CT to inspect the full volume of the cultural heritage objects [11]. The general requirements for the image processing technique implementations are to achieve selective information extraction by enhancement of contrast in the required grey-level bandwidth

at high computing speeds and to be transferrable across different radiographic image systems and modalities [12, 13].

There are many different methods for contrast enhancement of industrial radiographic images e.g. convolution-based methods and Gabor filtering [14-19].

Poisson Image Editing, PIE, is a simple gradient domain method that eliminates the non-uniform of pixel grey-level intensities whilst preserving image feature details. Poisson Editing is a gradient-based image editing because it solves the Poisson equation in the general form of $\Delta f = \text{div}(g)$, where g is the processed gradient. The basic approach of PIE is to find the best approximation function for a given vector in the L_2 -norm and to impose its high-pass filter. The advantages of PIE are that it has a single contrast parameter and it is flexible in that it can be applied to images across most imaging modalities and conditions [20-21]. A detailed discussion on this method could be found in section 3.3.

2. Research aim

The aim of this research is to reveal the hidden structure and damaged regions in the ancient sculptures by the radiography testing and image processing method. For this purpose, PIE was used for selective information extraction from digital radiographic images of art objects for fog removal and enhancement of contrast in ROI (region-of-interest). The image processing method was applied to radiographs of four valuable sculptures acquired at the Radiographic Inspection Laboratory (RIL), University Institute for the Restoration of Heritage of the Universitat Politècnica de València.

3. METHODS

3.1. Specifications of sculptures

Radiographs of the four sculptures were selected from the many acquired over the past two decades and held in RIL archives. The selection was based on the size, material, and technique used in their construction as well as the presence of internal features of interest from a restoration/preservation and radiographic viewpoint.

Fig.1 shows photographs of the sculptures to which the radiographs belonged and included, *Child Jesus*, *Puppet head belonging to Francisco Sanz Baldoví. S. XIX*, *The Christ Child as Salvator Mundi*, *Christ* and *Skinned Man*. The sculptures were made in different materials including wood, paper, and wax, and provided a suitable variation from the radiographic and image processing viewpoint.

From an image acquisition viewpoint, the whole of the object should be covered within a single image which means the X-ray focal point to object distance needs to be large. To achieve acceptable X-ray uniformity, however, the field-of-view needs to be reduced which would therefore allow imaging of only smaller objects.

For larger objects, especially when using conventional films, it may be necessary to cover the whole object with two or three radiographs. This can be achieved by several radiography experiments, where the source and detector are moved. The software of our film digitizer system can scan several films and combine them by the edges to a single image file. So a single digit is generated for each specimen.

For digital radiography cases, our setup allows us to use a larger field of view, and thus we can obtain the whole object in a single shot. Of course, it again depends on the object size, detector size, and field of view of the X-ray tube.

Decreasing the object to the X-ray detection/acquisition plane allows for imaging of larger objects for the same image geometric size but as well as requiring a larger field-of-view and therefore decreasing the field uniformity, leading to the detection of proportionately more scattered radiation and hence noisier images. Sculpture selection was therefore made to include the above effects within the scope of the study: of the four sculptures, therefore, *Child Jesus*, *Puppet head*, and *The Christ Child as Salvator Mundi* were medium sizes, *Christ* was larger and the *Skinned Man* was of a life-size, see Table 1.

The sculpture construction techniques used by the artist, *Child Jesus*, *Puppet head*, and *The Christ Child as Salvator Mundi* were multi-material which is common in the RIL collection. *Christ* was chosen as an example of a sculpture crafted in a glued-paper technique referred to as *cartapesta* or *papelón*, developed during the Spanish Baroque period between the 16th and 18th centuries. The figure of *Skinned Man* was made in wax, a more uncommon material used in the period, and was usually crafted in academies of medicine or fine arts from the 18th century [22].

From the conservation point of view, all these pieces present similar internal features including fractures, possible damage caused by xylophages, or the presence of metallic elements. In addition, the radiographic imaging revealed other structural elements such as glass-eyes and internal metal fastening elements. Such information is of significance in restoration and preservation procedures on art objects since most externally visible deterioration originates from internal deterioration.

The radiography-guided intervention [5] on each sculpture was to resolve specific issues for each sculpture as indicated in Table 1 which included lack of balance of the sculpture, loss of grip on top of the sculpture with increased risk of toppling, and damage.

3.2. X-radiography procedure

The radiographs had been acquired using a system, with a TRANSPORTIX-50 X-ray tube manufactured by General Electric with a potential voltage range of 20kV to 110kV, 2mm aluminum filter, a focal spot size of 2.3 mm for X-ray tube, and a current of 20mA. The half-angle of the Field-of-view was almost 20 degrees as was indicated by a light field.

The images from *Child Jesus* were acquired using conventional radiographic film whilst the images of the other items were acquired using digital radiography, ~~therefore,~~ also the image of the Puppet head was made by both conventional and digital radiography, allowing some comparison of the two different imaging systems.

The film radiographs were acquired using Structurix D7 by Agfa which had yielded fine grain and high contrast images. The digital images for the other three sculptures had been acquired using a CR MDT4.OT chassis from the same company in combination with a standard general-purpose CR plate.

The exposure time had been adjusted to enable a plain level field for the inter technique comparisons, that is the exposure time for the images from the *Child Jesus*, was 1 minute and 10 seconds whilst the digital image acquisition exposure times were only about three seconds.

The radiograph from *Child Jesus* was digitized using an Imacon Flextight 646 digitizer which was very different from the images from the CR plates which were read using the 4.0T CR with dimensions of 350mm by 430mm and a resolution of 3480×4248 pixels a spatial resolution of about 100 microns

To overcome the issue of comparing images of two different radiography systems with different dimensions of the detector (Film or CR plate) and to enable direct comparison between the two sets of images obtained from the two different systems, the

RIL routine from CR EASYLIFT (also from the Agfa) allowed sequential sweeps of the entire image.

It was, therefore, possible to form complete images from the two different acquisition systems i.e. with their maximum bit-depth resolution and 16-bit grayscale [5]. The total set of images is arranged as a mosaic to form the complete image. X-ray that will retain its maximum bit-depth resolution, through its 16 bits/channel in its grayscale mode. The images were thus available in DICOM format and a mosaic form of the complete image for further processing.

As a further step, the images were transformed into TIF format, downgrading them to 8 bits and converting them to an RGB color space. The above operations facilitated the processing of the images whilst in practice did not compromise the outcome of the study. Of course, in some cases, 16-bit image has to be implemented for a more precise investigation. It will use more computational time and needs faster CPUs or GPUs.

Depending on the size and the elemental composition of the objects, the X-ray potential was increased to enable sufficient penetration of the photons to achieve the required statistical precision of the pixel values [8, 23]. Table 2 shows a summary of the radiography settings for each of the sculptures.

3.3. Poisson image editing (PIE) method

In this study, to reduce the blurriness, detect defects and improve the contrast of radiographs, we consider a gradient-domain model and obtain its solution using Fourier Transform. We begin by introducing the desired gradient-domain model. Let f be the given noisy function (or f is the noisy image with $M \times N$ dimensions). The main goal of the gradient domain model is finding the function (image) u such that its vector gradient

be close to the vector gradient of f and also has lower variance in comparison with f .

Therefore, analogous with [21], in this paper, we consider the following gradient model:

$$\min_u \int_{\Omega} \|\nabla u - \nabla f\|^2 dx + \lambda \int_{\Omega} (u - \bar{u})^2 dx \quad (1)$$

where “guidance vector field” ∇f is defined in closed subset Ω [24], \bar{u} denotes the mean value, and the constant $\lambda > 0$ is a regularization parameter that controls the trade-off between the data fidelity term $\int_{\Omega} \|\nabla u - \nabla f\|^2 dx$ and the regularization term $\int_{\Omega} (u - \bar{u})^2 dx$ in equation (1). The solution to the cost function was obtained using the following Screened Poisson Equation with a homogeneous Neumann boundary condition [21, 24]:

$$\begin{cases} \lambda u - \Delta u = -\Delta f, & \text{in } \Omega \\ \frac{\partial u}{\partial \mathbf{n}} = 0, & \text{in } \partial\Omega, \end{cases} \quad (2)$$

where \mathbf{n} is the normal vector to the boundary and $\partial\Omega$ is the boundary of Ω . For $\lambda > 0$, equation (2) has a unique solution.

There are several methods for solving (2), or equivalently (1), but in this paper, we implement a Fourier-based method to obtain the desired solution. In [22, 24], one solution for (2) in spatial domain is derived as follows

$$u(x, y) = f(x, y) - \left(\frac{1}{2\pi} K_0(\sqrt{\lambda(x^2 + y^2)}) * f(x, y) \right), \quad (3)$$

where “*” denotes the convolution operator and $K_0(r)$ is the zeroth-order modified Bessel function of the second kind and defined as follows [25-26]

$$K_0(r) = \int_1^{\infty} \frac{e^{-rt}}{\sqrt{t^2-1}} dt. \quad (4)$$

Therefore, as it can be seen in (3), the solution u is the difference between the given function f and its blurred version which is convolved with kernel K_0 . From a different point of view, equation (3) acts as a background removal strategy. Indeed, in the background removal strategy, first, the background of an image is computed, and then, to obtain the enhanced image, it will be subtracted from the original noisy image, see [27] and [28] for more details.

To explicitly compute the solution u in (3), like [21], we use Discrete Fourier Transform (DFT). It is shown that one can impose implicitly the Neumann boundary condition by extending the original image symmetrically across its sides. In this situation, we obtain an image that is four times bigger and also is symmetric and periodic. Therefore, for a $J \times L$ grid, the solution of the screened Poisson equation (2) in the Fourier domain can be computed as follows

$$\hat{u}_{mn} = \frac{\left(\left(\frac{2\pi m}{J}\right) + \left(\frac{2\pi n}{L}\right)\right)}{\left(\lambda + \left(\frac{2\pi m}{J}\right)^2 + \left(\frac{2\pi n}{L}\right)^2\right)} \hat{f}_{mn}, \quad (5)$$

where \hat{f} denotes the DFT of the given image f . To obtain solution u , it is sufficient to apply discrete inverse Fourier transform on (5).

In Algorithm 1, we briefly describe the required steps to obtain the solution of Screened Poisson Equation (2). As it can be seen in Algorithm 1, we applied a Simplest Color Balance [3] with saturation parameter s before and after processing, see [21, 25-26]. Indeed, to deal with outliers, the Simplest Color Balance saturates a certain percentage of the image's bright pixels to white and dark pixels to black. The saturation level is an adjustable parameter that affects the quality of the output. We set $s = 2$ in our experimental results.

Algorithm 1: The background removal strategy with a gradient-domain method

1. Inputs

- a. Input given noisy image f
 - b. Input the regularization parameter $\lambda > 0$
 - c. Input the percentage of saturation s
 2. Processing
 - a. Balance the input image f with $s\%$ saturation
 - b. Apply the discrete Fast Fourier transform on the f and obtain \hat{f}
 - c. Evaluate the solution of Screened Poisson Equation in Fourier domain and obtain \hat{u}
 - d. Apply the discrete inverse Fourier transform to obtain u
 - e. Balance the image u with $s\%$ saturation
 3. Output
 - a. The enhanced sharp image u .
-

The algorithm was executed in an Ubuntu–Linux environment with an Intel Core-i7 based workstation.

The evaluation of the practical value-added to archaeological assessment and conservation procedures by the image processing method described above was made by presenting the outcomes to experienced operators.

This was carried out by level-II radiography certificate holders, restorers, and archaeologists. A scoring scale was used for each image in the range of 5 to 1 with 5 for excellent, 4 for very good, 3 for good, 2 for bad, and 1 very bad. The final scores were averaged and represented in percentage form.

4. RESULTS AND DISCUSSION

Fig. 2 shows the radiograph of the *Child Jesus* sculpture; see Fig.1-a for the corresponding photograph. The conventional film radiograph shows features corresponding to signs of fracture on the surface of the object. The fundamental reason for the acquisition of the radiographic image was however to utilize information to aid in the evaluation and repair of its internal features/damage. The acquired radiograph was found however to be

somewhat foggy which masked fine internal detail hindering the evaluation procedure; the PIE algorithm was applied with a few to target contrast enhancement.

It has to be noted that the blurring affecting an image acquired with a low- resolution and low-contrast detector is less evident than for a detector with high-resolution detector such as D4 radiography film. Of course, the resolution of the film scanner is also very important in the case of conventional radiography films. So when using high resolution and/or high contrast detectors, blurriness of the image is became very important.

CR and DR can provide higher contrast in comparison with conventional radiography films. According to digital radiography standards, if a high contrast image can be provided, it can also help for increasing the spatial resolution, which is called the compensation principle in digital radiography [29-30]. The spatial resolution of radiography films can be better than CR or DR systems. However, for our test, the spatial resolution is not our first priority, because we are not dealing with fine cracks in our samples.

Usually, the contrast of images is very important for cultural heritage objects. For our cases, the spatial resolution of the CR system can be up to 50 microns, but 100 microns was selected. This spatial resolution is enough for our samples and also it reduces the amount of data.

The effectiveness of the proposed algorithm relies on the optimization of λ which poses a challenge since it is dependent on the level of foginess present in the radiograph. It was found that large values of λ lead to a highly smoothed image that is in effect a representation of the foggy component of the image (Fig.3). This component was then subtracted from the original radiographs yielding the sharper reconstructed image shown in Fig. 4. Close examination of the two images showed that the reconstructed image

revealed the details of the object's internal structure, patterns, and design more effectively with sharper feature edges as highlighted by the arrows on the two figures. From a restoration viewpoint, the accuracy of determining the position of previously placed metal nails and screws enabled the insertion of additional nails and screws with more confidence and avoidance of overlaps.

Fig. 5 a and c show the radiographs of Puppet head, belonging to Francisco Sanz Baldoví. S. XIX. (Fig1-b) by film and CR. Fig.5-c and d show the enhanced images by the PIE algorithm for $\lambda=0.003$. It can be seen that PIE can increase the detectability of different parts specifically in the jointing points of the Puppet head (please refer to the figure marks). The details of images can be viewed better by the CR system and PIE method.

Fig. 6 shows the CR image of the *Christ*, see the photograph of Fig.1-c. The reason for electing to radiograph the object was to reveal how the sculpture had been fixed to the base with a view also to determining any associated damage/decay of wood.

The position of where separate pieces had been joined to form the sculpture, for example, the joining of the crown to the head, the attachment of the hands to the body, and the foot of the sculpture to the wooden cross, was visualized in the radiographic images as shown in Figs. 6-a. Figs. 6-c and e show magnified images of the head and hand regions and the corresponding processed reconstructed images are shown in Figs.6-b, c and f. Comparison of the two sets of images showed that the internal structure, locations of joints, and the position of cracks and fractures inside are visible with higher contrast once the fogginess was removed.

Fig.7-a and Fig.7-b show the original radiographs and PIE processed images associated with different parts of the sculptures, *The Christ Child as Salvator Mundi* and *Skinned Man*; see Fig.1-d and Fig.1-e for the corresponding photos. The internal

structure, the wood carving in the head areas, and the location of nails were identifiable in the original radiographs. The corrosion of wood and nails embedded in the head was however better visualized in the reconstructed image Fig.7-b. Also, some of the cavities could be recognized in the head section as identified by arrows.

The radiograph and the reconstructed image of the *skinned man* are shown In Fig.7-c and Fig.7-d. The fixation bar, the muscle, bones, and body parts could be seen in different parts of the sculpture. The shaping wax used for sculpting the muscle, bones, and joints is better to define in the reconstructed image, especially in the ear and skull regions.

Table 3 shows the scores of the radiography and restoration experts' evaluations in percentage terms. The processed images have been evaluated by five experts, the total score for an image is 25, and therefore, the score values in percentage values are given as:

$$\text{the score values in percentage values} = \frac{\text{the sum of the points given by the experts}}{\text{the total score}} \times 100$$

The data showed that high scores were given to the original radiographs but in the feature boundaries, the reconstructed images performed better.

The preference of the reconstructed images was due to clearer visualization of the internal structures where improvement to the imaging contrast had been made. The experts also conveyed that the extent and the nature of the fractured regions and fixing nails were also better visualized in the reconstructed images. The runtimes of the PIE algorithm were between about 5 and 7 seconds on a PC with an Intel Core-i7 microprocessor running in an Ubuntu Linux environment.

It is known that each image processing method is based on a mathematical algorithm. Some different features can be extracted by the different methods with the

change of their parameters that different parameters that the output results are influenced by the choice of parameters. In this study, we try to use the PIE method with a background removal algorithm that is independent of parameter selection by the user. For comparison, a convolution Gaussian method and a FFT method were implemented to Fig. 2 dependent on the chosen parameter by the user.

In Fig.8-a and 8-b, the result of outputs is shown for discrete Gaussian convolution and Fast Fourier transform (FFT) for sharpening the radiography images. Each filter has different parameters and must be adjusted by the user. The best results from the change of the parameters depend on the required extracted feature. There are very useful methods with many parameters that may have similar results such as Fig.8 as well as the PIE method.

Fig. 9 shows line profile plots for the images of Figs. 2, 4-c, and 8. The Line profile evaluation was used to determine image quality enhancement with the application of PIE due to different algorithms. To further evaluate the performance and compare of the PIE algorithm with some other methods such as the Gaussian convolution and FFT methods, the profiles in the path of elongated AB in Fig. 2 for the original radiography, Fig. 4-c for PIE and Fig. 8 for two mentioned algorithms were studied. Let us consider the edges as a benchmark. All three processing methods showed the edges clearer with respect to the original radiograph. PIE and the Gaussian methods are in the same order and much better regarding FFT and the original image. Please note the line profile has a small shift in the X direction to avoid overlapping in the graphs.

5. CONCLUSION

The results showed that the PIE method was effective in selective region enhancement of

the radiographic image contrast enabling better visualization of the objects' internal structures. Conservators and radiographers were able to improve the visualisation of the sculptures' internal features and achieved enhanced evaluation visualization which improved the restoration procedures. The speed, of the processing algorithm, enables short evaluation and intervention times.

REFERENCES

- [1] J. Lang, and A. Middleton, *Radiography of Cultural Material*, 2nd edition, Elsevier Butterworth-Heinemann, Oxford, 2005.
- [2] J. Langlois, G. Mary, H. Bluzat, A. Cascio, N. Balcar, Y. Vandenberghe, and M. Cotte, 'Analysis and conservation of modern modeling materials found in Auguste Rodin's sculptures', in *Studies in Conservation*, **62**(5) (2016) 247–265, DOI: 10.1080/00393630.2015.1131029
- [3] O. Schalm, L. Vanbiervliet, P. Willems, and P. De Schepper, 'Radiography of paintings: Limitations of transmission radiography and exploration of emission radiography using phosphor imaging plates', in *Studies in Conservation*, **59**(1) (2014) 10–23, DOI: 10.1179/2047058413Y.0000000088
- [4] P. Jett, S. Sturman, and T. D. Weisser, 'A study of the Egyptian bronze falcon figures in the Walters art Gallery', in *Studies in Conservation*, **30**(3) (1985), 112–118, DOI: 10.1179/sic.1985.30.3.112
- [5] J. A. Madrid, 'Use of telemetry x-ray techniques in large-size pictorial works', in *Ge-conservation*, **5** (2013) 101–109.
- [6] M. Castelle, M. Bormand, Y. Vandenberghe, and D. Bourgarit, 'Two of a Kind: Shining New Light on Bronze Spiritelli Attributed to Donatello', in *Studies in Conservation*, **65**(4) (2020), 200–211, DOI: 10.1080/00393630.2019.1655261
- [7] E. Negahdarzadeh, E. Yahaghi, B. Rokrok, A. Movafeghi, and A. Keshavarz Khani, 'Diagnosis of design and defects in radiography of ceramic antique objects using the

wavelet-domain hidden Markov models’, in *Journal of Cultural Heritage*, **35** (2019) 56–63.

[8] J. A. Madrid, ‘Dos décadas de inspección radiográfica en España: retrospectiva y horizontes futuros en un contexto de cambio tecnológico’, in *Intervención*, **10** (2014) 87–95.

[9] F. Casali, ‘X-ray and Neutron Digital Radiography and Computed Tomography for Cultural Heritage’, in *Physical Techniques in the Study of Art, Archaeology and Cultural Heritage*, ed. by D. Bradley, D. Creagh, Elsevier, Amsterdam, (2006) 41–123.

[10] E. Yahaghi, M. Mirzapour, A. Movafeghi, P. Mohammadi Matin, and B. Rokrok, ‘FISTA Algorithm for Radiography Images Enhancement with Background Blurring Removal’, in *Research in Nondestructive Evaluation*, **30**(2) (2019) 80–88. DOI: 10.1080/09349847.2018.1476744

[11] M. P. Morigi, F. Casali, M. Bettuzzi, R. Brancaccio, and V. D’Errico, ‘Application of x-ray Computed Tomography to Cultural Heritage diagnostics’, in *Appl Phys A* **100** (2010) 653–661, DOI: 10.1007/s00339-010-5648-6

[12] B. Wedvika, M. Steinb, J. M. Stornesc, and J. Mattssond, ‘On-site Radioscopic Qualitative Assessment of Historic Timber Structures: Identification and Mapping of Biological Deterioration of Wood’, in *International Journal of Architectural Heritage: Conservation, Analysis, and Restoration* **10**(5) (2015) 646–662, DOI: 10.1080/15583058.2015.1077905

[13] M. Bettuzzi, R. Brancaccio, F. Casali, S. Cornacchia, M. Gior-dano, M. P. Morigi, A. Pasini, and D. Romani, ‘Innovative systems for digital radiography and Computed Tomography: applications for Cultural Heritage diagnostics’, in *Physics Methods in Archaeometry*, ed. by M. Martini, M. Milazzo, M. Piacentini, IOS Press, Amsterdam, (2004) 461–470.

[14] P. Getreuer, ‘A Survey of Gaussian Convolution Algorithms’, in *Image Processing On Line* **3** (2013) 286–310.

[15] J. Canny, ‘A computational approach to edge detection’, in *IEEE Transactions on Pattern Analysis and Machine Intelligence* **8** (1986) 679–698.

- [16] K. R. Rao, and J. Ben-Ariem, 'Lattice architectures for multiple-scale Gaussian convolution, image processing, sinusoid-based transforms and Gabor filtering', in *Analog Integrated Circuits, and Signal Processing* **4**(2) (1993) 141–160, DOI: 10.1007/BF01254865
- [17] G. Amayeh, A. Tavakkoli, and G. Bebis, 'Accurate and efficient computation of Gabor features in real-time applications', in *Advanced in Visual Computing, Lecture Notes in Computer Science*, **5875** (2009) 243–252, DOI: 10.1007/978-3-642-10331-5_23
- [18] W. Forstner, and E. Gulch, 'A fast operator for detection and precise location of distinct points, corners, and centers of circular features', in *Proc. ISPRS Intercommission Conference on Fast Processing of Photogrammetric Data.* (1987) 281–305. Interlaken, Switzerland.
- [19] D. G. Lowe, 'Distinctive image features from scale-invariant key points', in *International Journal of Computer Vision* **60**(2) (2004) 91–110.
- [20] J. M. Di Martino, G. Facciolo, E. Meinhardt-Llopis, "Poisson Image Editing", *Image Processing On Line*, (2016), <https://doi.org/10.5201/ipol.2016.163>
- [21] Morel, J.M., Petro, A.B. and Sbert, C., 2014. Screened Poisson equation for image contrast enhancement. *Image Processing on Line*, 4, pp.16-29.
- [22] J. A. Madrid, 'Aplicación de la técnica radiográfica digital en el estudio de Bienes Culturales. Caso de estudio de un Desollado', in *Asociación Española de Ensayos No Destructivos* **61** (2012) 10–17
- [23] J. A. Madrid, 'Catálogo radiográfico del servicio de rayos x del Laboratorio de Documentación y Registro', in *Arché* **8-10** (2015) 87–97
- [24] J.M. Morel, A.B. Petro, and C. Sbert, Fourier implementation of Poisson image editing, *Pattern Recognition Letters*, 33 (2012), pp. 342 – 348.
<http://dx.doi.org/10.1016/j.patrec.2011.10.010>.
- [25] N. Limare, J.L. Lisani, J.M. Morel, A.B. Petro, and C. Sbert, Simplest Color Balance, *Image Processing On Line*, (2011). <http://dx.doi.org/10.5201/ipol.2011.llmps-scb>.

[26] Abramowitz, Milton, Irene A. Stegun, and Robert H. Romer. "Handbook of mathematical functions with formulas, graphs, and mathematical tables." (1988): 958-958.

[27] Yahaghi, Effat, Mahdi Mirzapour, Amir Movafeghi, Parisa Mohammadi Matin, and Behrouz Rokrok. "Fista algorithm for radiography images enhancement with background blurring removal." *Research in Non-destructive Evaluation* 30, no. 2 (2019): 80-88.

[28] Mirzapour, Mahdi, Effat Yahaghi, and Amir Movafeghi. "The performance of three total variation based algorithms for enhancing the contrast of industrial radiography images." *Research in Non-destructive Evaluation* 32, no. 1 (2021): 10-23.

[29] Training course series no. 60, Guidelines on Training, Examination and Certification in Digital industrial radiology testing (RT-D), International Atomic Energy Agency (IAEA), Vienna, 2015.

[30] ISO-17636 part 2, Non-destructive testing of welds -Radiographic testing -Part 2: X- and gamma-ray techniques with digital detectors, International Standard organization, Geneva, 2013.

Tables and figures legends

Table 1. Characteristics of sculptures and the reason for doing radiography.

Table 2. Radiography settings for each sculpture.

Table 3. The averaged percentage of given points by the expert of radiography and restoration for each sculpture (See the text).

Fig. 1 the photography images the chosen sculptures a) *Child Jesus* b) *Puppet head* c) *The Christ Child as Salvator Mundi* d) *Christ* and e) *Skinned Man*

Fig. 2 a typically radiograph of the he Child Jesus sculpture

Fig.3 The subtracted images of the *Child Jesus* sculpture

Fig. 3. The output images for a) $\lambda=0.003$ b) $\lambda=0.03$ c) $\lambda=3$

Fig. 4 the enhanced image: the output images (Fig.3) are subtracted from the original radiograph (Fig.2) for a) $\lambda=0.003$ b) $\lambda=0.03$ c) $\lambda=3$

Fig. 5. The radiograph of Puppet head, belonging to Francisco Sanz Baldoví. S. XIX. (fig1-b) by a) film, b) CR, c and d) the enhanced images by PIE algorithm for $\lambda=0.003$

Fig.6 The original radiograph of the *Christ* sculpture (Fig.1-b), a) the whole body, c) the radiograph of head and e) hand regions b, d, f) their subtracted images for $\lambda=0.003$.

Fig.7 a,c) The original radiographs and b, d) the reconstructed images with $\square=0.003$ of Fig.1-c and d (The Christ Child as Salvator Mundi and the Skinned Man sculptures) for $\square=0.003$.

Fig. 8 result of a) a Gaussian convolution and b) fast Fourier transform (FFT) methods implemented to Fig. 2

Fig. 9 The plotted profiles in the DIQI AB line for the original radiograph (Fig.2), PIE method (Fig. 4-a); and Gaussian convolution and FFT methods (Fig.8- a, b)

Table 1 Characteristics of sculptures and the reason for radiography aided intervention

Name	dimensions (cm)	material	challenge
<i>Child Jesus</i>	52.0 × 23.0 × 23.0	Poly-material wood	Finding the best location of the screw
<i>Puppet head</i>	48.0 × 20.0 (max), 5.0 (min) × 22 (max)	Poly-material wood	Identification of the internal structure
<i>Christ</i>	110.0 × 84.0 × 12.0	Paper (<i>Cartapesta</i> technique)	Identification of the internal structure
<i>The Christ Child as Salvator Mundi</i>	69.0 × 43.0 × 40.0	Poly-material wood	Fixing to the base
<i>Skinned Man</i>	170.0 × 60.0 × 60.0	Wax	The consolidation problem in the middle zone

Table 2. Radiography settings for each sculpture.

Name	Voltage (kV)	Current (mA)	Exposure time (seconds)*	Source to subject distance (cm)	N° Plates	Detector (type)
<i>Child Jesus</i>	54	20	70	230	1	Structurix D7 (Film, industrial type)
<i>Puppet head</i>	45	20	75	100	1	Structurix D7 (Film, industrial type)
<i>Puppet head</i>	45	20	3	100	1	CR MDT4.0T (CR of GP Type)
<i>Christ</i>	45	20	3	260	6	CR MDT4.0T (CR of GP Type)
<i>The Christ Child as Salvator Mundi</i>	72	20	3	270	6	CR MDT4.0T (CR of GP Type)
<i>Skinned Man</i>	60	20	3	480	33	CR MDT4.0T (CR of GP Type)

* The exposure time per record.

Table 3. The averaged percentage of given points by the expert of radiography and restoration for each sculpture (See the text).

name	Score (%)	
	The original radiograph	The PIE reconstructed images
<i>Puppet head</i>	90%	95%
<i>Puppet head</i>	94%	99%
<i>Child Jesus</i>	92%	97%
<i>Christ</i>	89%	98%
<i>The Christ Child as Salvator Mundi</i>	88%	96%
<i>Skinned Man</i>	96%	100%



a



b



c



d



e

Fig. 1 the photography images the chosen sculptures a) *Child Jesus* b) *Puppet head* c) *The Christ Child as Salvator Mundi* d) *Christ* and e) *Skinned Man*

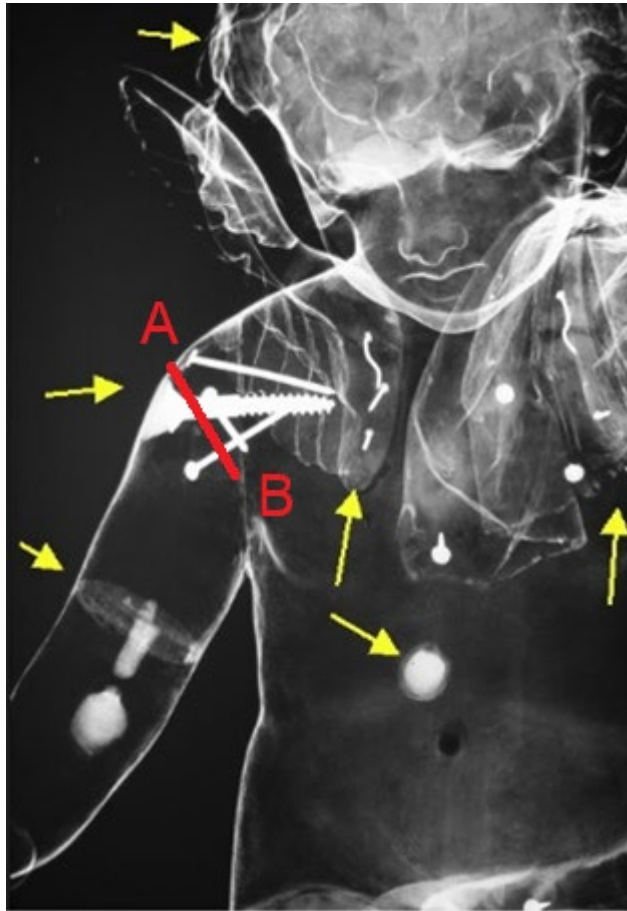


Fig. 2

Fig. 2 a typically radiograph of the he Child Jesus sculpture

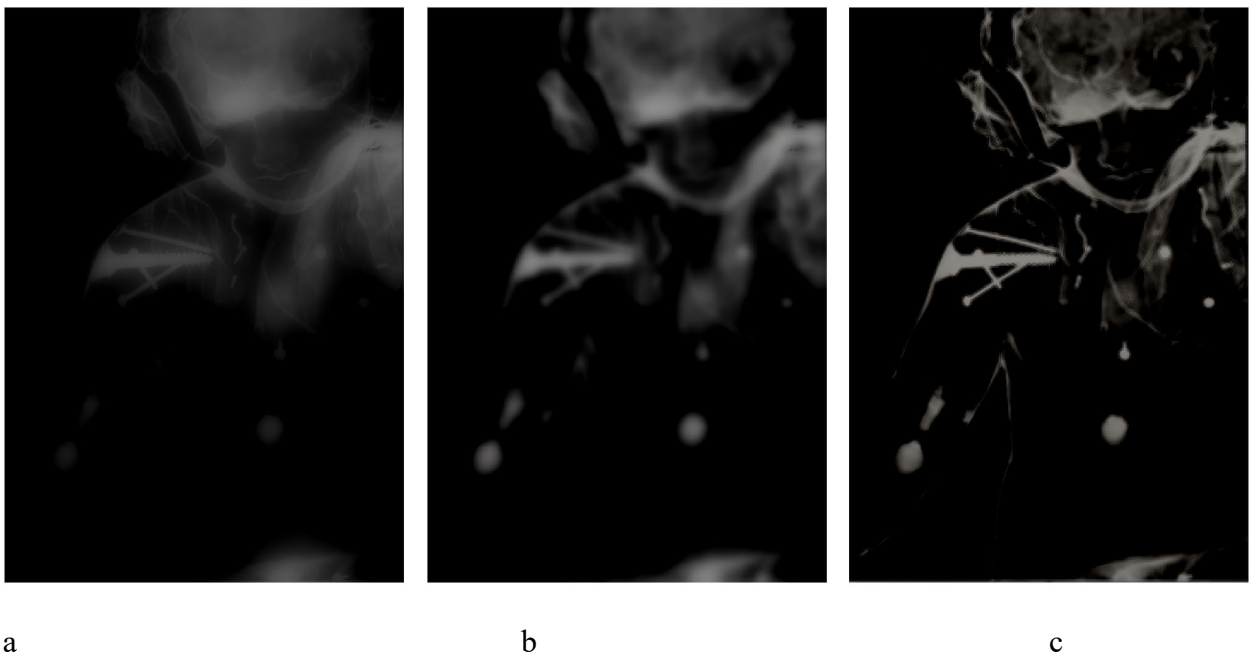


Fig. 3. The output images for a) $\lambda=0.003$ b) $\lambda=0.03$ c) $\lambda=3$

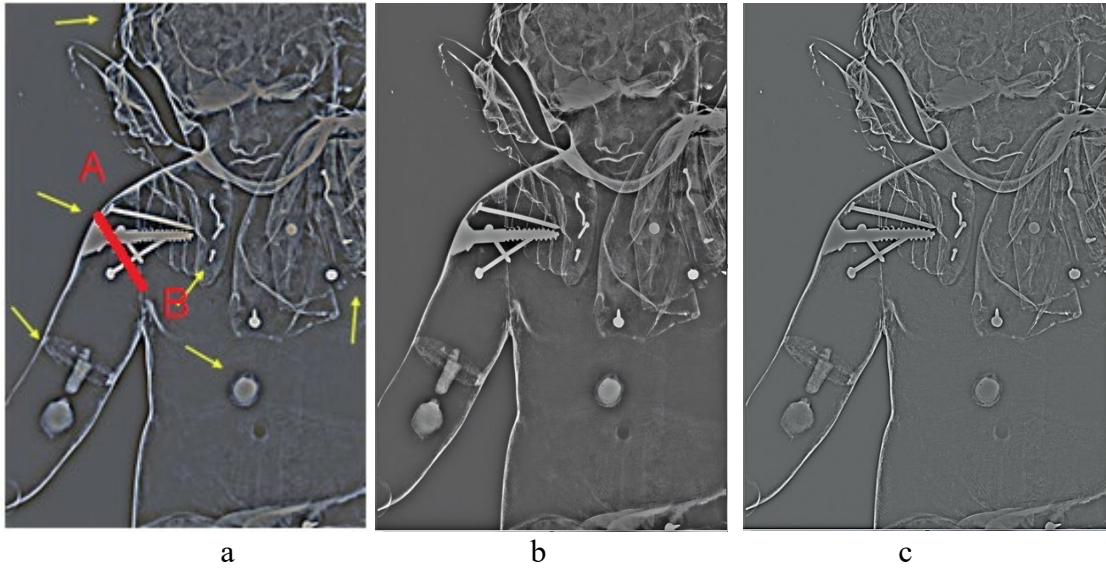


Fig. 4. the enhanced image: the output images (Fig.3) are subtracted from the original radiograph (Fig.2) for a) $\lambda=0.003$ b) $\lambda=0.03$ c) $\lambda=3$

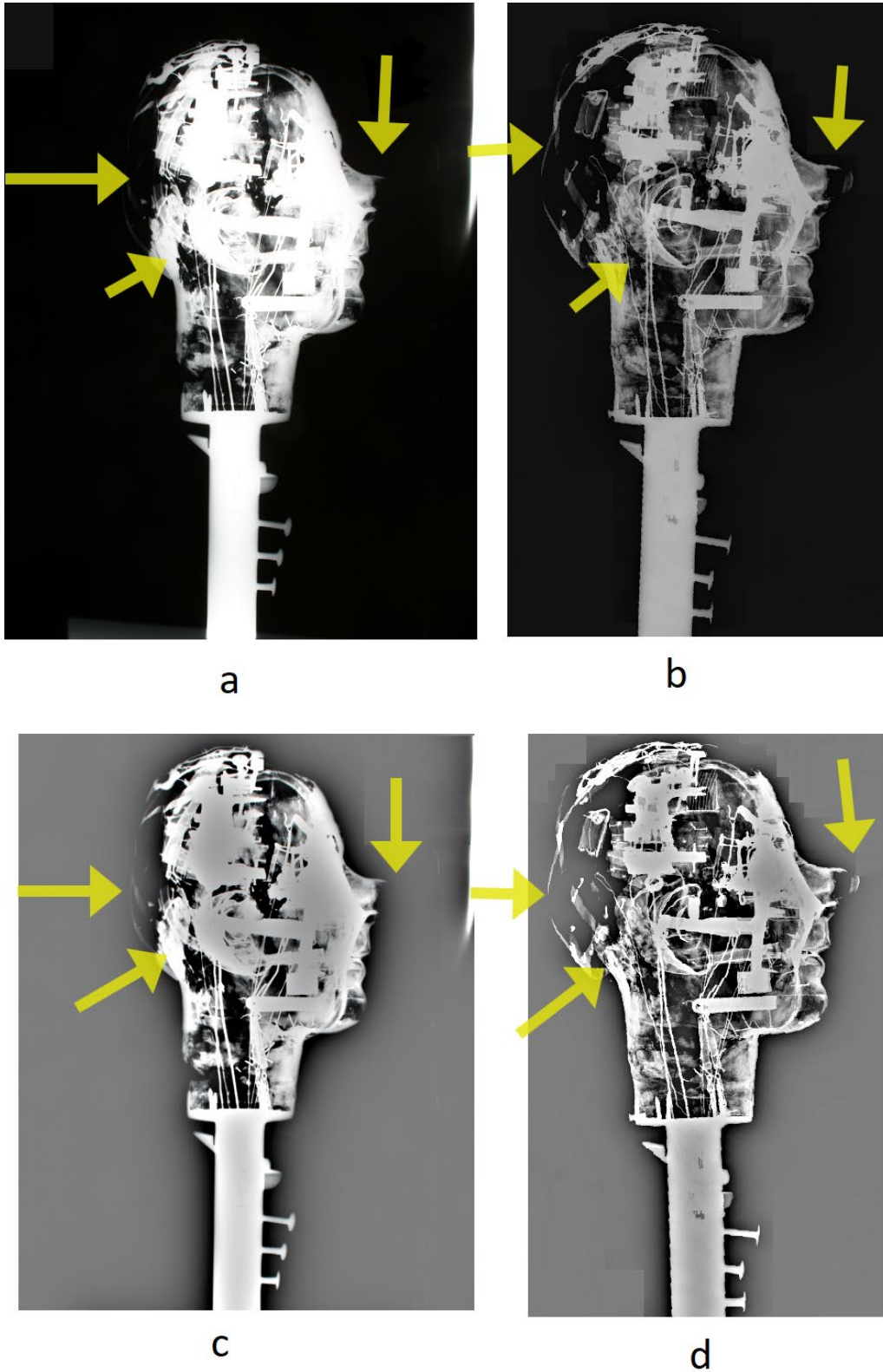
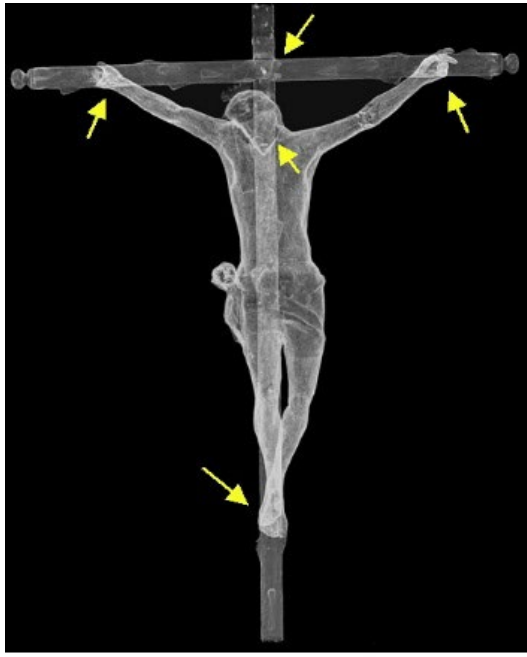
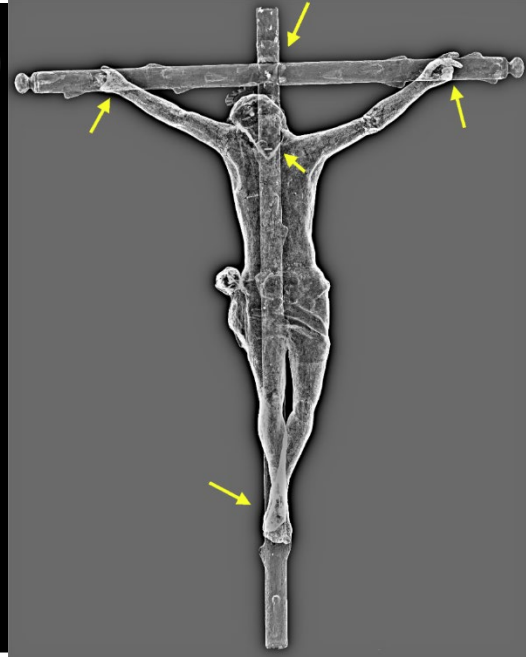


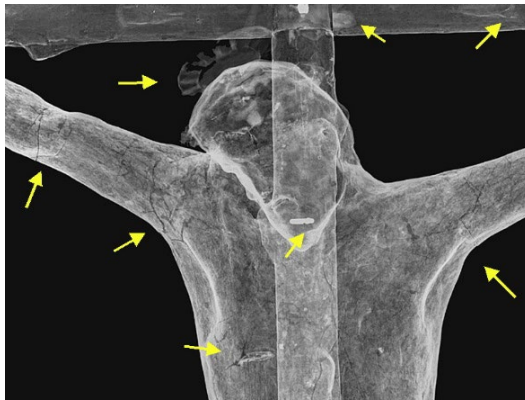
Fig. 5. The radiograph of Puppet head, belonging to Francisco Sanz Baldoví. S. XIX. (Fig1-b) by a) film, b) CR, c and d) the enhanced images by PIE algorithm for $\lambda=0.003$



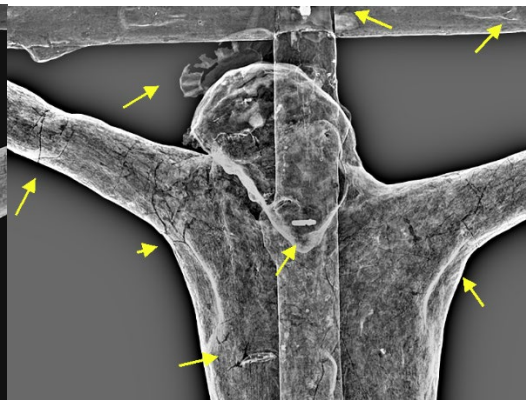
a



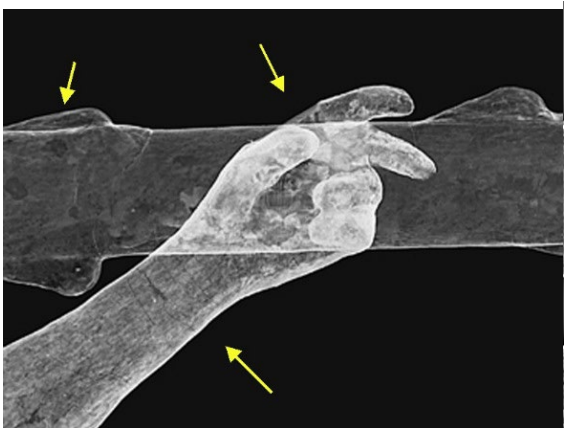
b



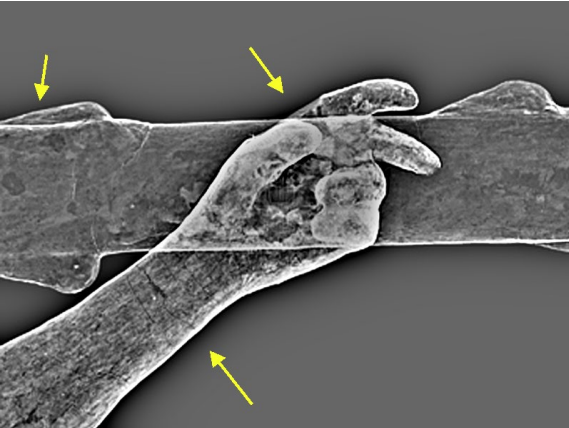
c



d



e



f

Fig.6 The original radiograph of the *Christ* sculpture (Fig.1-b), a) the whole body, c) the radiograph of head and e) hand regions b, d, f) their subtracted images for $\lambda=0.003$.

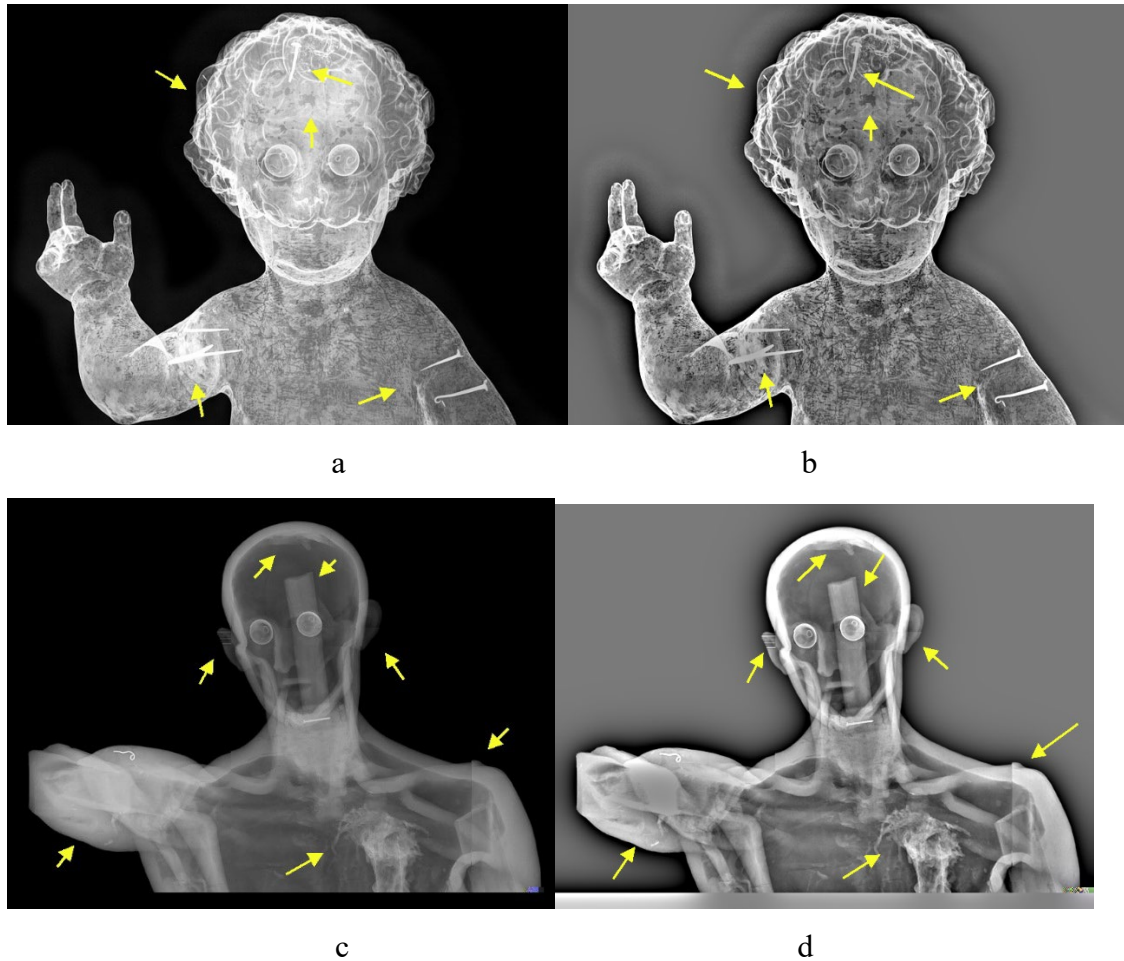


Fig.7 a,c) The original radiographs and b, d) the reconstructed images with $\lambda=0.003$ of Fig.1-c and d (*The Christ Child as Salvator Mundi* and the *Skinned Man* sculptures) for $\lambda=0.003$.

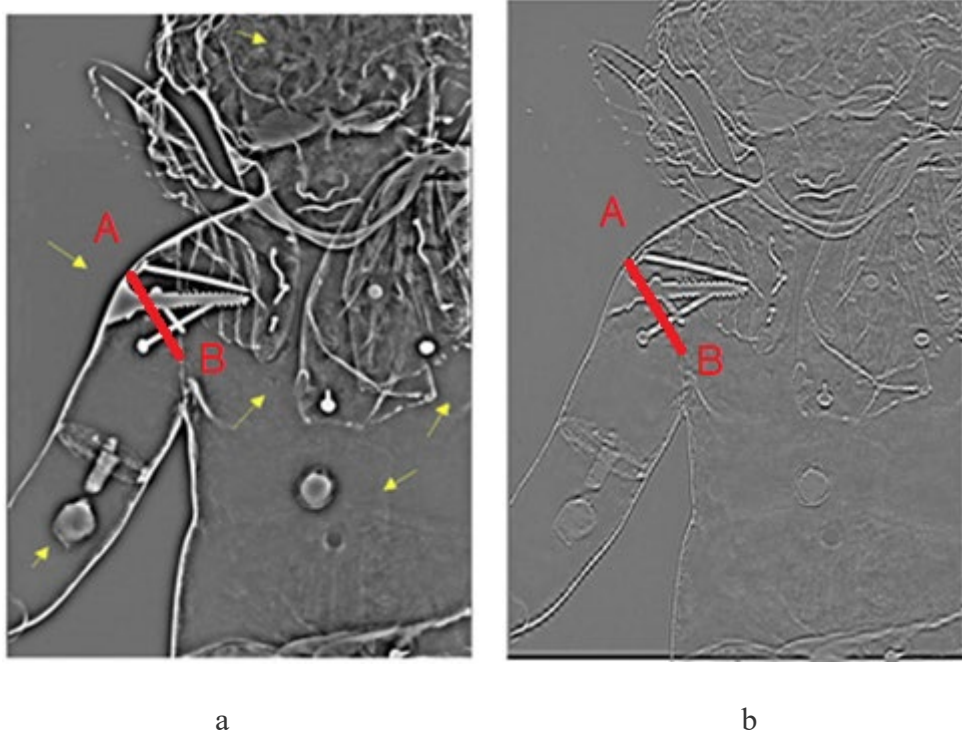


Fig. 8 result of a) Gaussian convolution and b) fast Fourier transform (FFT) methods implemented to

Fig. 2

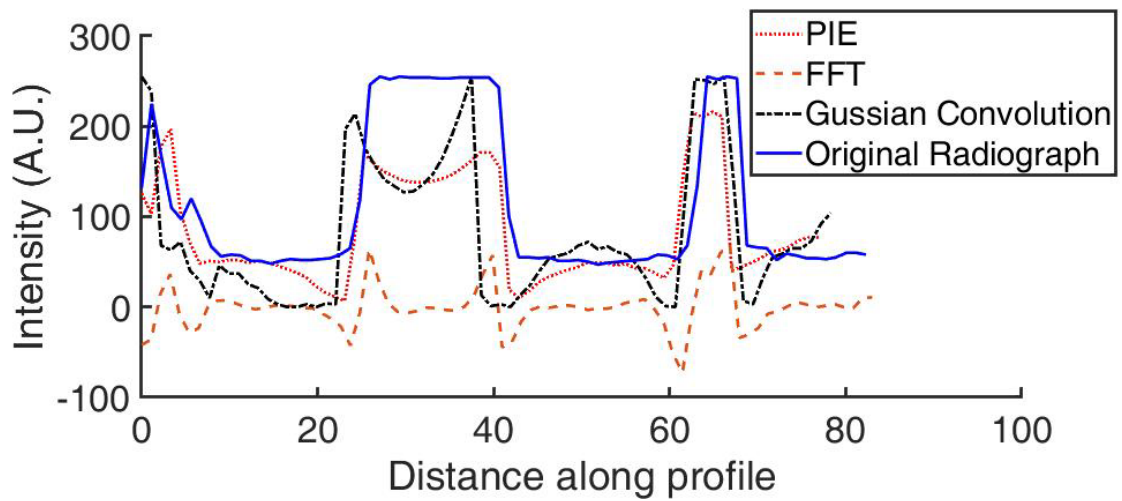


Fig. 9 The plotted profiles in the AB line for the original radiograph (Fig.2), PIE method (Fig. 4-a); a and Gaussian convolution and FFT methods (Fig.8- a, b)

